nature electronics

Article

https://doi.org/10.1038/s41928-024-01121-3

Ready-to-transfer two-dimensional materials using tunable adhesive force tapes

In the format provided by the authors and unedited

Table of contents

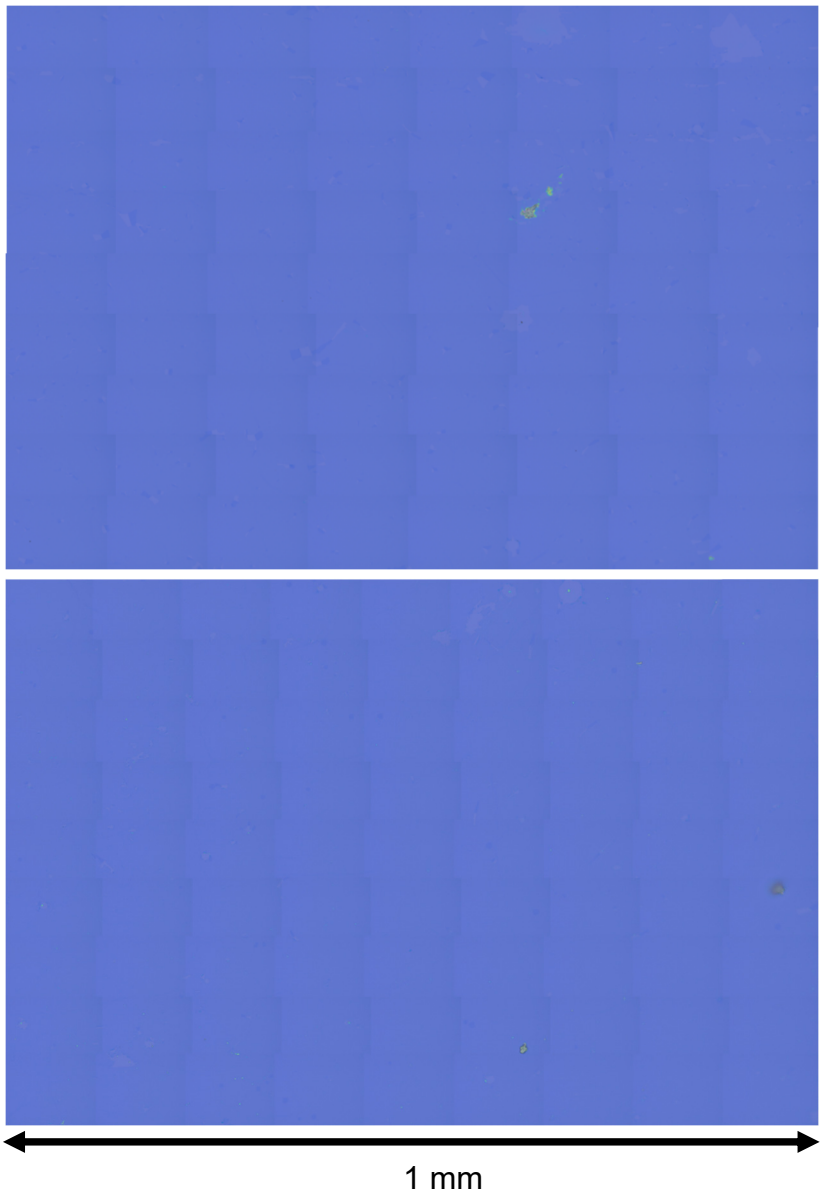

Supplementary Fig. 1. Transferred monolayer graphene sheet. Stitched optical images of monolayer graphene after the transfer on a SiO_2/Si substrate. Two different positions of one substrate are indicated. The transferred film is almost free from structural defects for large area.

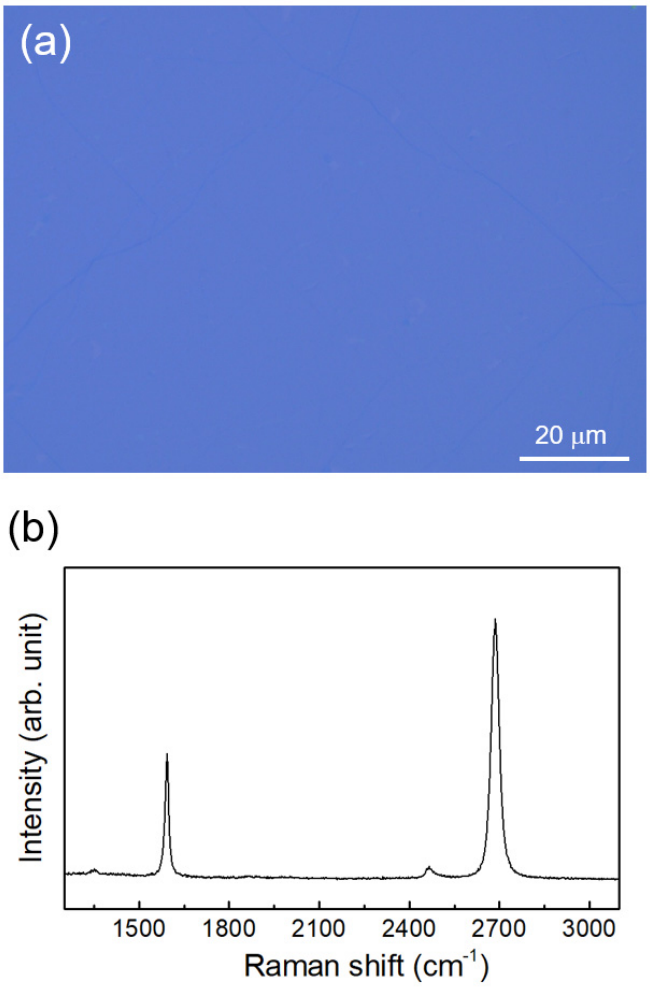

Supplementary Fig. 2. UV tape transfer of monolayer graphene from Cu foil. a, Optical image of the transferred monolayer graphene from electropolished Cu foil. **b**, Raman spectrum of the transferred graphene.

Supplementary Fig. 3. UV tape transfer of bilayer graphene from Cu-Ni film. The BLG grown on a Cu-Ni(111)/sapphire substrate was transferred on a SiO_2/Si substrate using the UV tape. The surface of the transferred BLG is very clean without apparent breakages, indicating that the tape transfer is not limited to monolayer graphene nor Cu catalyst.

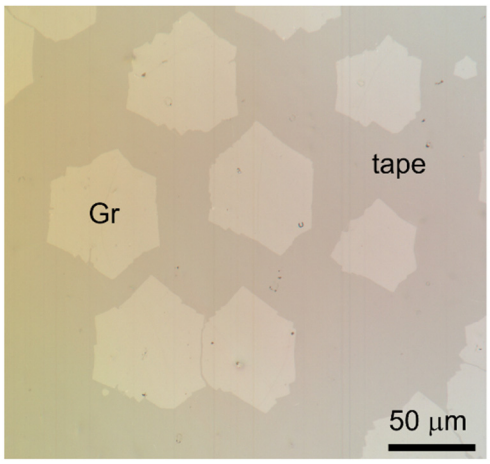

Supplementary Fig. 4. Monolayer graphene on the UV tape surface. Optical image of the UV tape surface with monolayer graphene grains on its top, measured with a laser microscope. This image shows the same graphene grains as those displayed in Fig. 1c,d, but the image is reversed because they are on the tape surface.

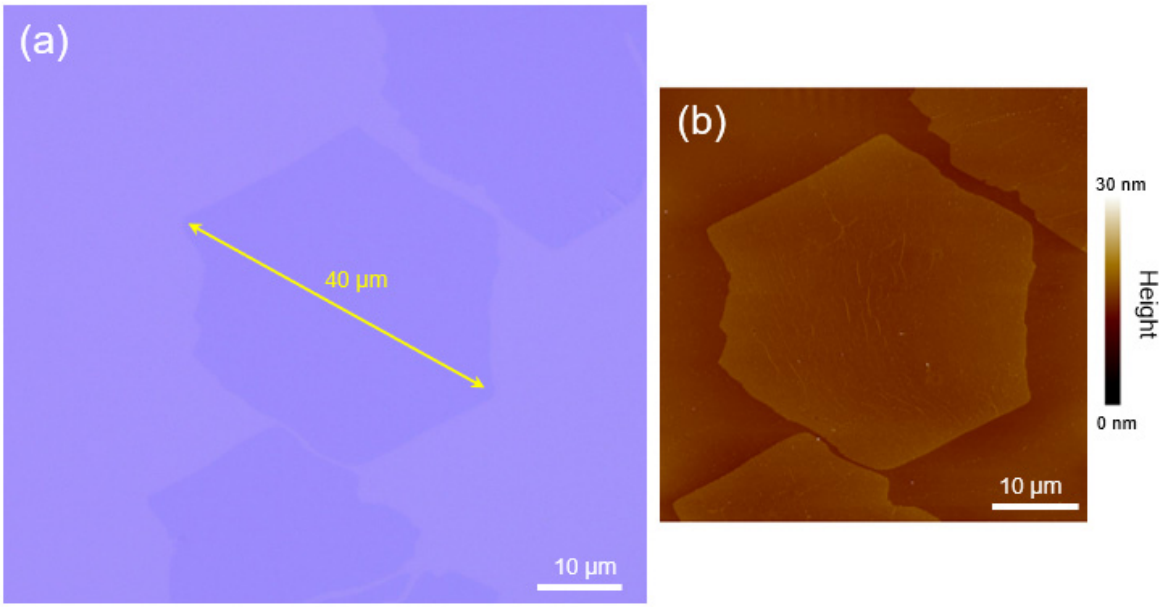

Supplementary Fig. 5. Transferred single crystal monolayer graphene grains. Optical (**a**) and AFM (**b**) images for an identical, large hexagonal graphene grain transferred with a UV tape.

(a)

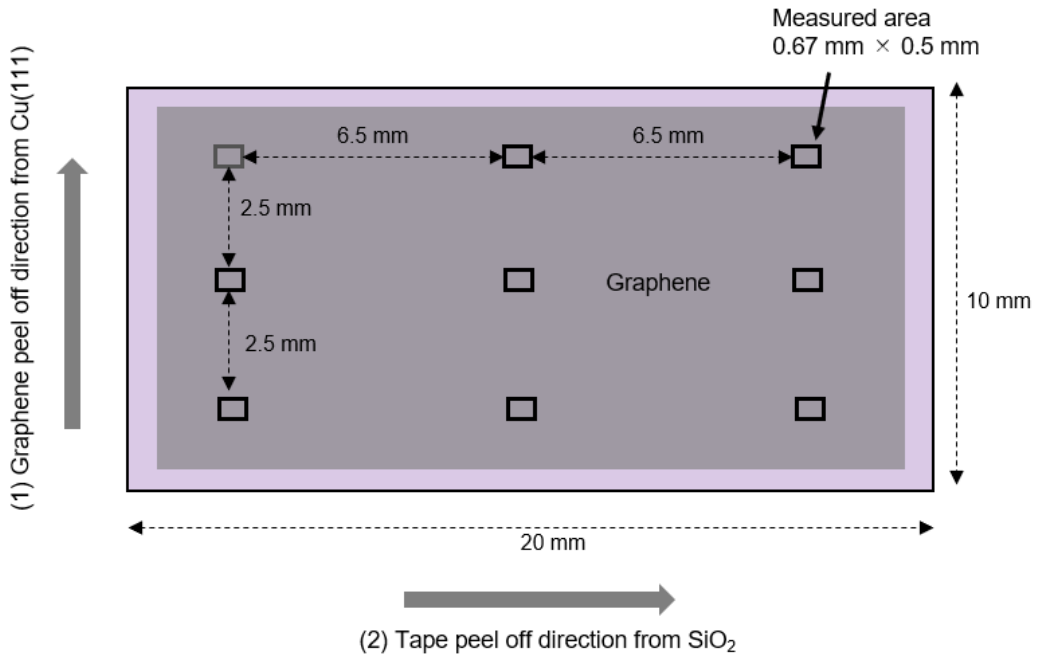

(b)

Batch number	Transfer yield (%)	Standard deviation
1	97.14	0.765
2	98.03	0.720
3	95.96	2.276
4	99.29	0.503
5	98.25	1.908
6	99.03	0.515
7	98.95	1.118
8	99.03	0.553
9	98.89	0.589
10	97.27	4.874
average	98.18	

Supplementary Fig. 6. Calculation of the transfer yield of monolayer graphene from Cu(111)/sapphire substrate. a, The nine measured areas in each batch to calculate the transfer yield. **b,** List of the average transfer yields obtained for each of 10 different transfer batches.

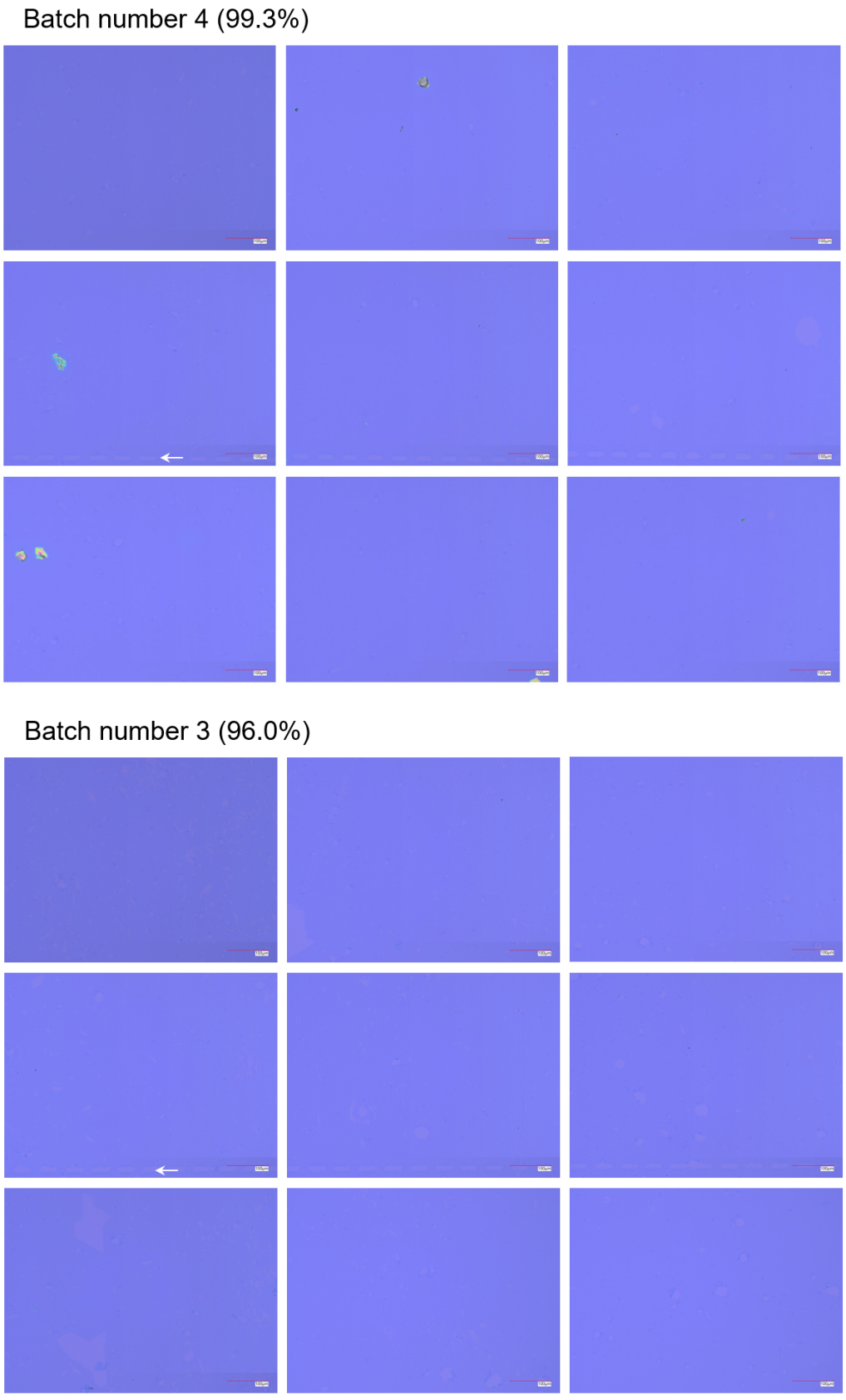

Supplementary Fig. 7. Optical images of the transferred graphene. Optical micrographs of two different batches with the highest (batch 4) and lowest (batch 3) transfer yields. White arrows in the middle panels show the marked patterns used to identify the measuring positions.

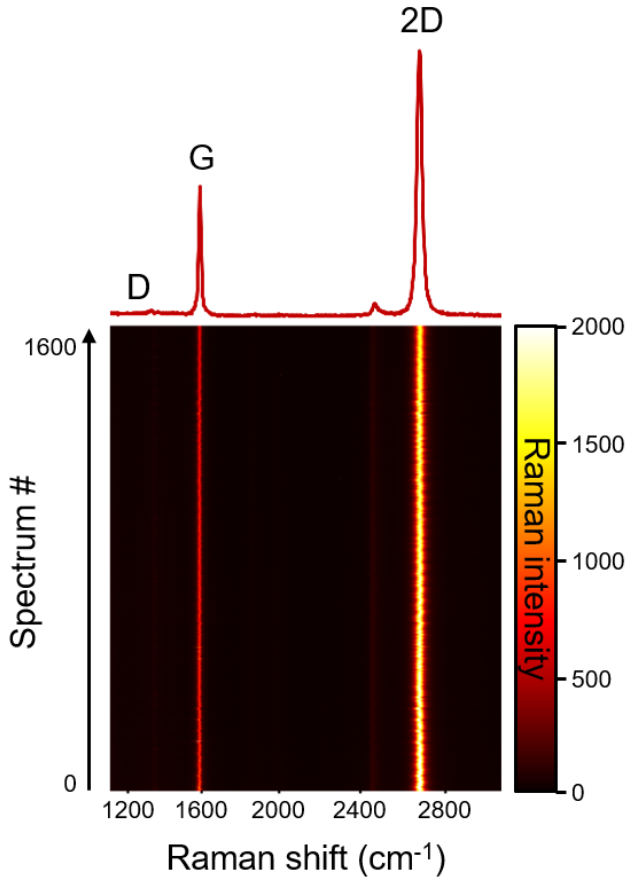

Supplementary Fig. 8. Raman peak intensity profile of transferred monolayer graphene. The 1600 Raman spectra for the area mapped in Fig. 1g of the main text are shown in this graph. This graph indicates a negligibly small D band and a high uniformity of the spectra in the whole area.

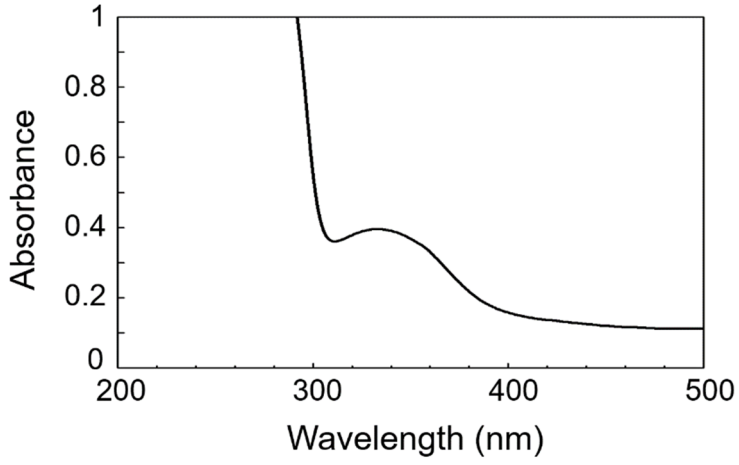

Supplementary Fig. 9. Optical absorption of the UV tape used for monolayer graphene. High optical absorbance at UV region indicates that the illuminated UV light is screened by the tape before reaching the graphene surface.

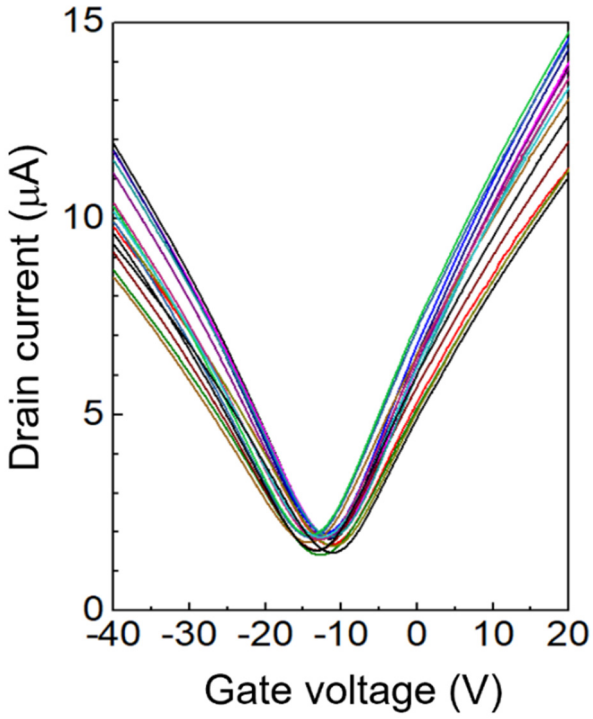

Supplementary Fig. 10. Transfer characteristic of graphene FETs. Representative transfer curves of different FETs fabricated with UV tape transferred monolayer graphene, measured in vacuum at room temperature. The devices showed uniform transfer characteristics, representing high-quality, clean transfer of the graphene sheets.

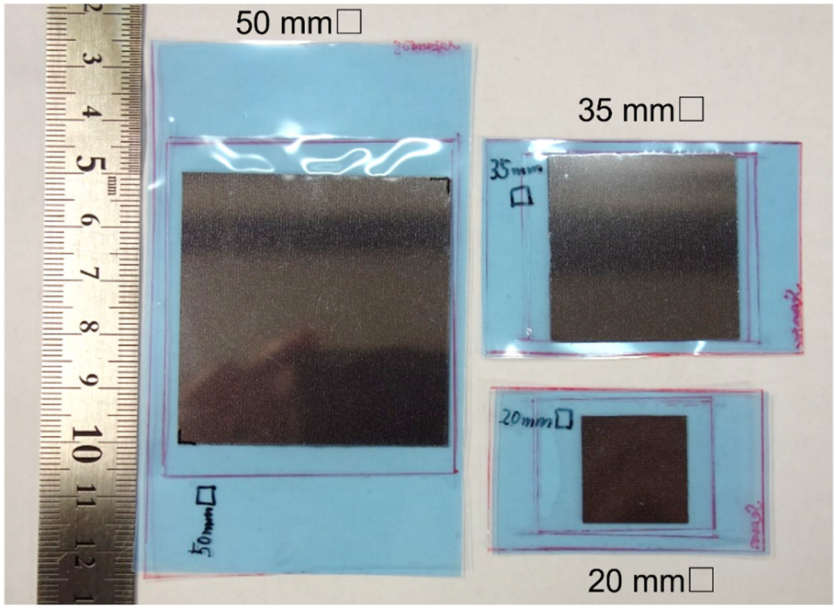

Supplementary Fig. 11. Three graphene/Cu(111) substrates with UV tapes, used for large-area three-layer stacked graphene. Three tapes were used to make the graphene stack shown in Fig. 1i of the main text. This photograph shows UV tapes attached to graphene/Cu(111)/sapphire substrates before the electrochemical delamination.

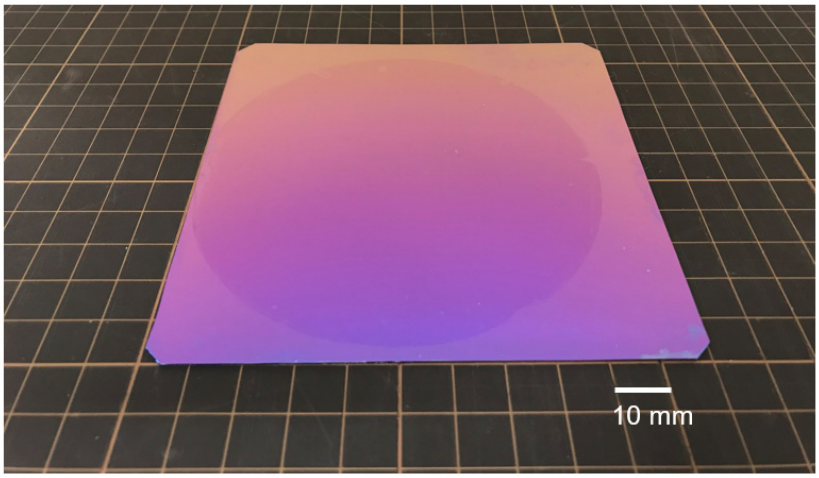

Supplementary Fig. 12. Large-area transferred graphene. Photograph showing the 4-inch monolayer graphene transferred on a SiO_2 substrate. Solid and robust UV tape allows the large-area transfer easier and more reliable.

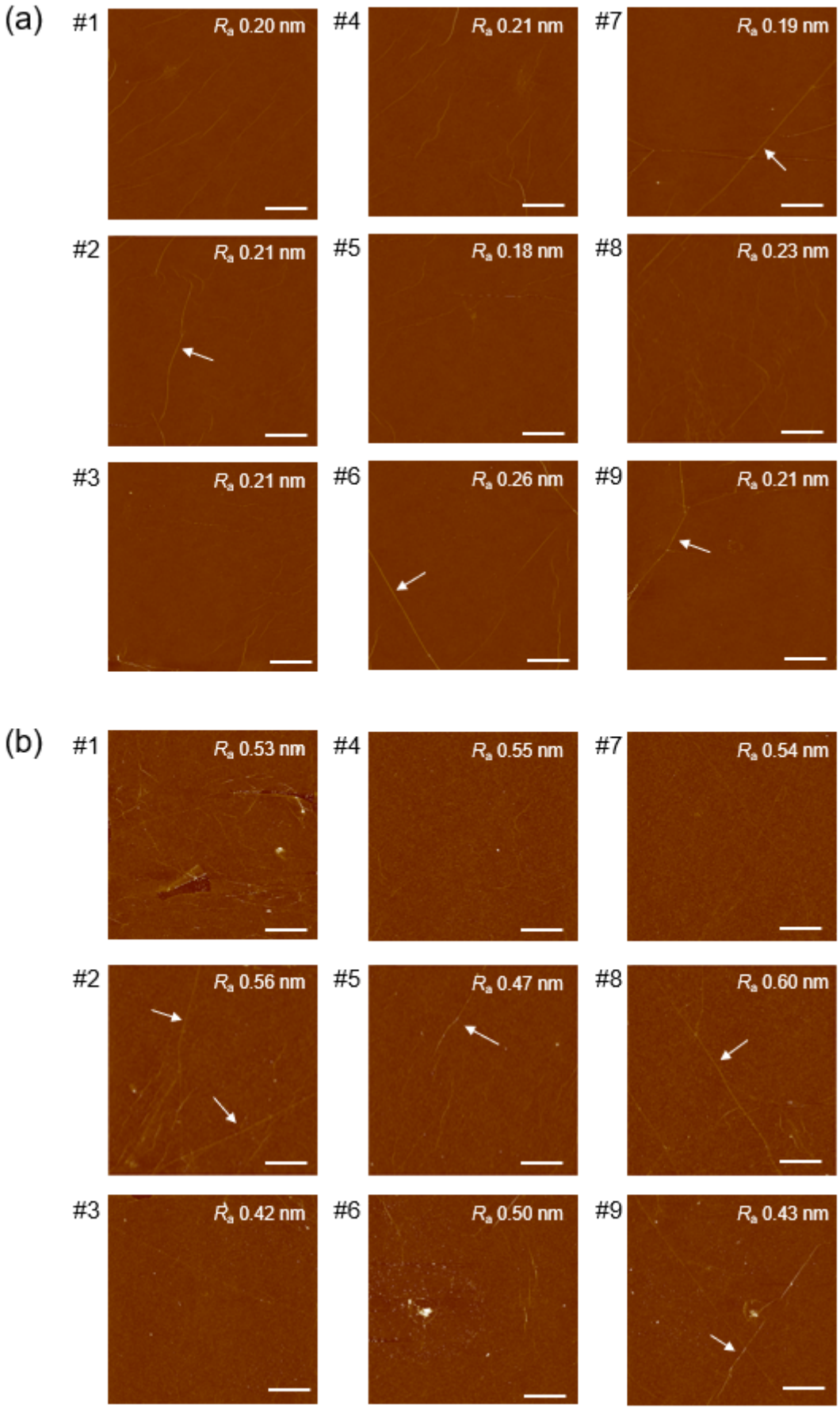
(a)
#1
R_a 0.20 nm
#4
R_a 0.21 nm
#7
R_a 0.19 nm
#2
R_a 0.21 nm
#5
R_a 0.18 nm
#8
R_a 0.23 nm
#3
R_a 0.21 nm
#6
R_a 0.26 nm
#9
R_a 0.21 nm
(b)
#1
R_a 0.53 nm
#4
R_a 0.55 nm
#7
R_a 0.54 nm
#2
R_a 0.56 nm
#5
R_a 0.47 nm
#8
R_a 0.60 nm
#3
R_a 0.42 nm
#6
R_a 0.50 nm
#9
R_a 0.43 nm

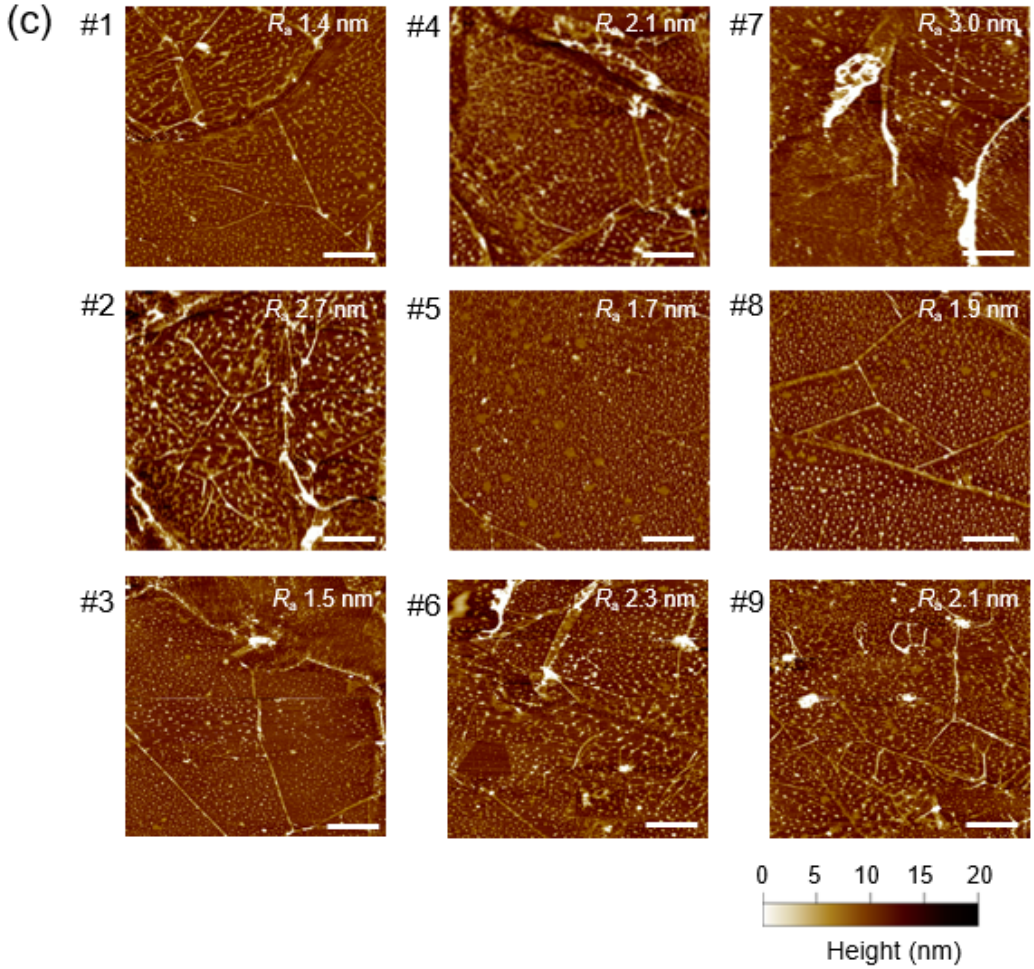

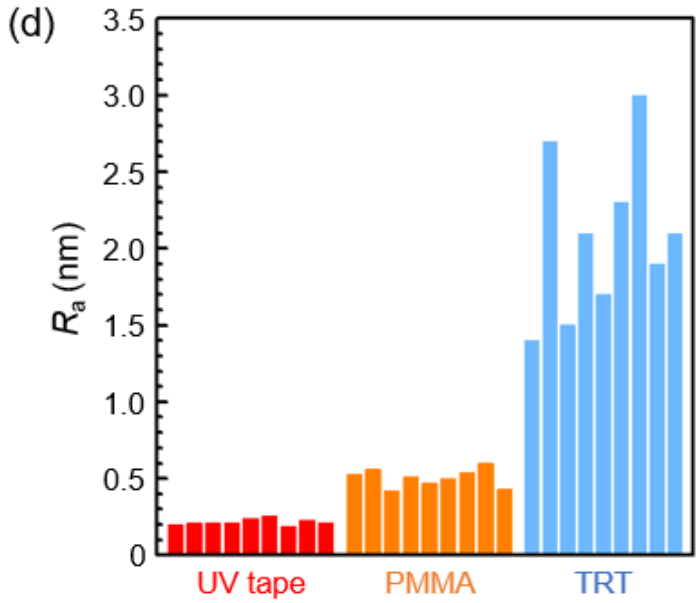

Supplementary Fig. 13. Comparison of AFM images and surface roughness of transferred graphene films. AFM images of monolayer graphene transferred by the UV tape (**a**), PMMA (**b**), and TRT (**c**), measured at nine different positions. In **a** and **b**, some of wrinkles

are highlighted with white arrows. All scale bars are 2 μm. **d**, R_a values of each transferred graphene.

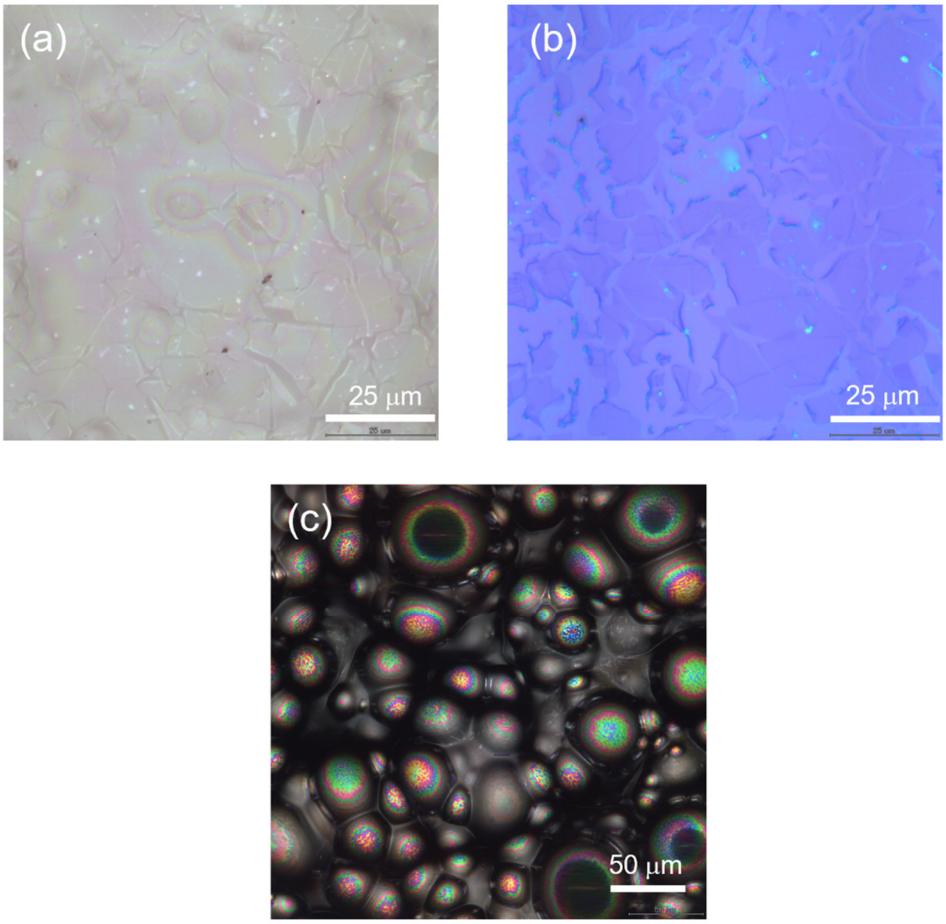

Supplementary Fig. 14. Transfer of monolayer graphene with TRT. a, Optical image of the TRT surface after the electrochemical transfer with graphene on the surface. **b**, Optical image of the graphene transferred with the TRT. **c**, Surface of the TRT after the graphene removal by the heat treatment. A number of foams are observed on the TRT surface, which contribute to the detachment from SiO_2 surface.

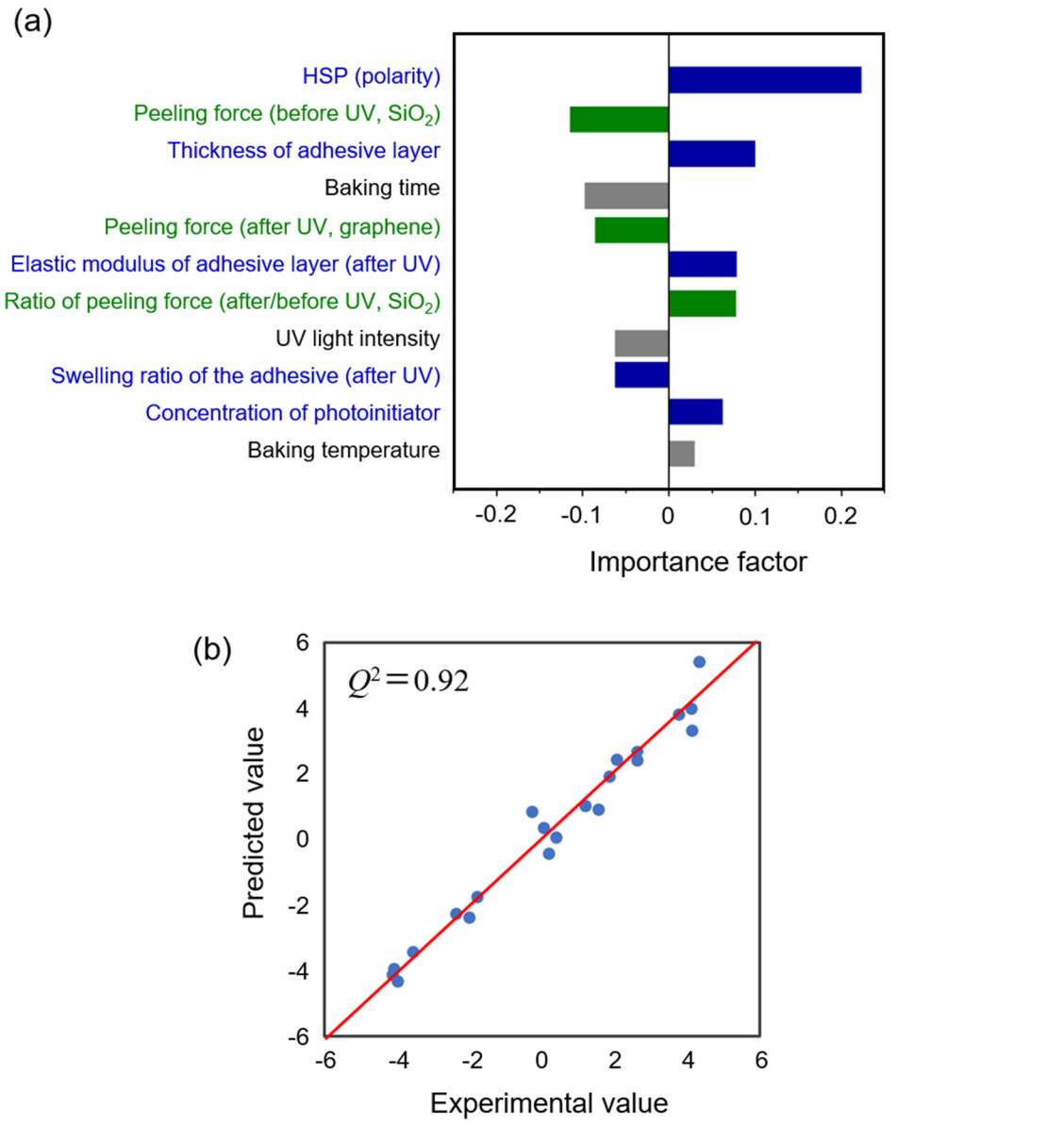

Supplementary Fig. 15. Machine learning-based development of the UV tape for the transfer of monolayer graphene. a, Importance factors of the tape characteristics and transfer conditions determined by examining 21 different tapes prepared in this research. We used least absolute shrinkage and selection operator (LASSO) method to calculate these values. A positive index indicates that a larger value is more effective for the successful graphene transfer, while a negative index indicates that a smaller value is more effective for the graphene transfer. The sum of the absolute importance factors is set 1.0. **b**, Comparison of the experimental values and predicted values (LASSO method). The values in the graph correspond to the logit functions of the graphene transfer yield.

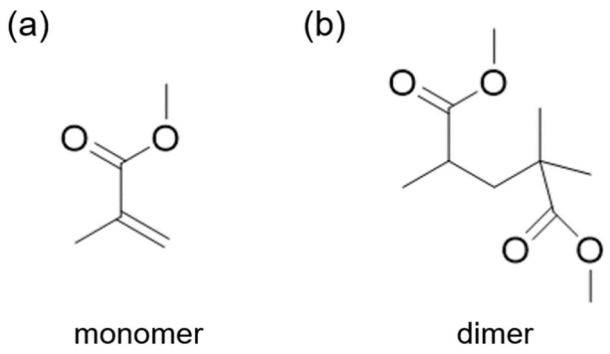

Supplementary Fig. 16. Chemical structures used for the DFT calculations. These chemical structures show the monomer and dimer used in the calculation (Fig. 3b,c).

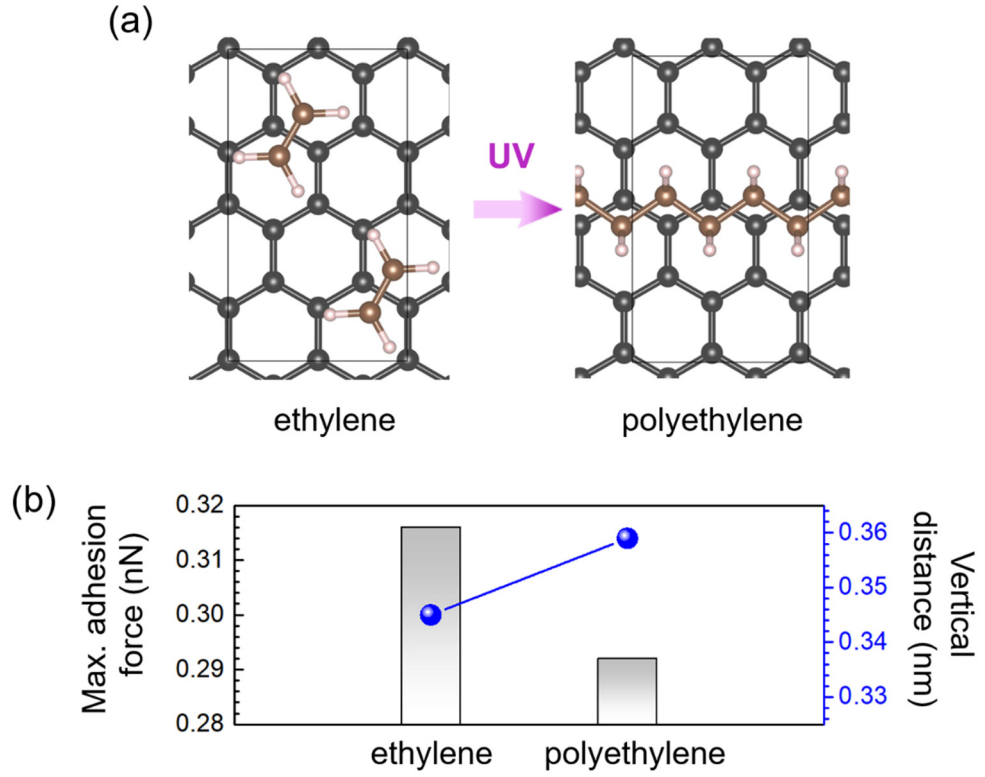

Supplementary Fig. 17. DFT calculation of the photo-induced polymerization of ethylene molecules. In addition to the dimerization reaction calculated in Fig. 3b-d, we also studied the polymerization reaction of ethylene on graphene surface. **a,** Atomic structures used to calculate the adhesion force of the UV tape to graphene. On the surface of graphene, ethylene molecules (left) are assumed to be polymerized to form polyethylene (right). **b**, Comparison of maximum adhesion force (gray) and vertical distance between graphene and the molecule/polymer (blue). Similar trend is observed with Fig. 3b-d.

The stable adsorption conformations of the adsorbates were found by calculating various adsorption conformations. The graphene surface in the unit cell for these calculations contained 16 C atoms with the lattice parameters set to 4.9 Å × 8.5 Å × 15.0 Å ($\alpha = \beta = \gamma = 90°$). A 4×4×1 Monkhorst-Pack *k*-point grid was chosen. The energy cutoff for the plane-wave basis set was set to 400 eV. Other calculation conditions are the same as those presented in the main text.

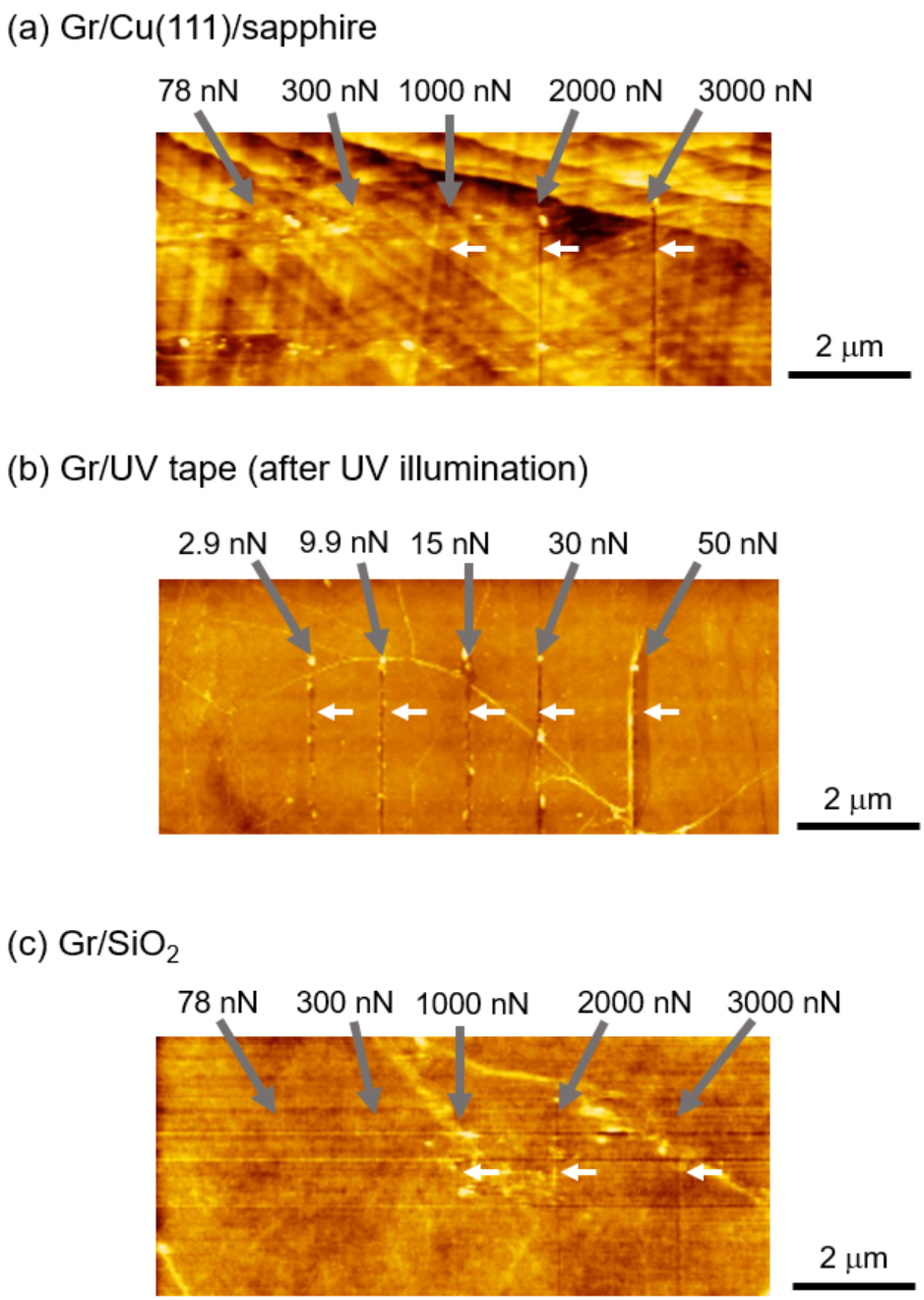

Supplementary Fig. 18. Adhesion force of monolayer graphene on different substrates. Monolayer graphene was scratched with a cantilever using FFM. The applied force to the cantilever is indicated with a gray arrow. White arrows show the formation of scratched lines in graphene, reflecting the adhesion force to each substrate. It can be seen that the graphene on the UV tape (after UV illumination) is very weak against the scratch. This indicates that the adhesion of graphene on the UV tape is much weaker than those of graphene on Cu(111) and SiO_2/Si substrates.

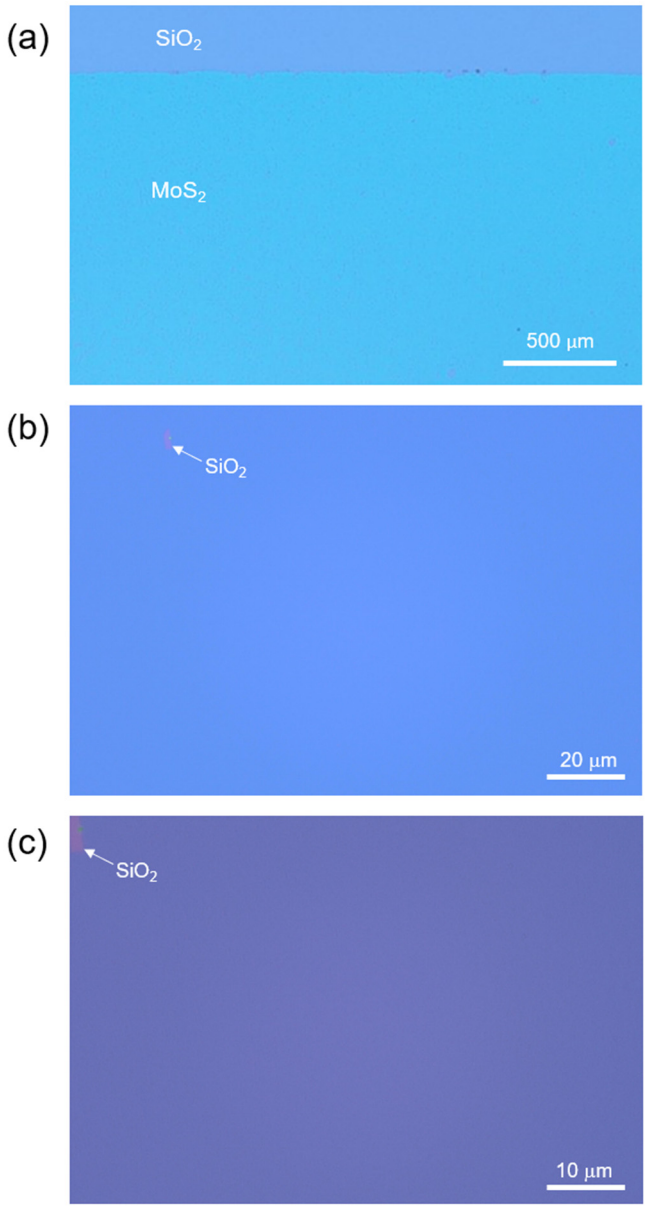

Supplementary Fig. 19. Optical micrographs the tape-transferred monolayer MoS_2 sheet. Optical microscope images of uniform monolayer MoS_2 which was transferred from sapphire using the UV tape. In **b** and **c**, we selected an area with a small pinhole to prove the presence of the monolayer MoS_2.

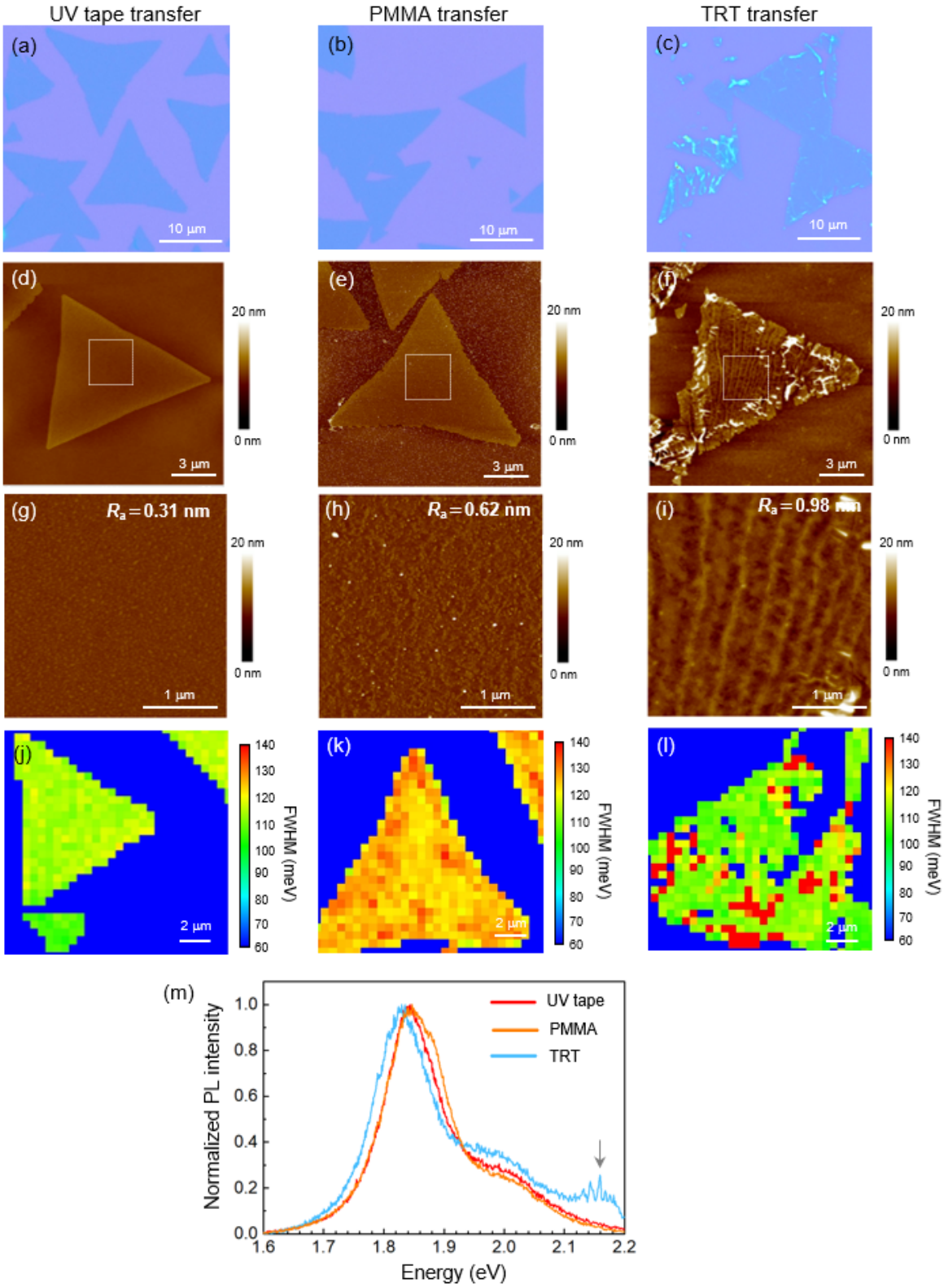

Supplementary Fig. 20. Comparison of MoS_2 grains transferred by the UV tape, PMMA, and TRT. Optical and AFM images of the UV tape- (**a**,**d**,**g**), PMMA- (**b**,**e**,**h**), and TRT-transferred (**c**,**f**,**i**) monolayer MoS_2 grains. The squares in **d**, **e**, and **f** indicate the imaging areas shown in **g**, **h**, and **i**, respectively. The UV tape transfer gives cleaner surface than the PMMA-

assisted transfer (as seen from their R_a values), while the TRT heavy contaminated the MoS_2 surface. Mapping of the FWHM of the PL peak taken from the UV tape- (**j**), PMMA- (**k**), and TRT-transferred (**l**) MoS_2 grains. **m**, Comparison of the normalized PL spectra. It is seen that the PL spectrum is slightly broader in the PMMA-transferred MoS_2 as compared with the tape transferred sample. The MoS_2 transferred with the TRT showed multiple peaks originated in tape residue (highlighted by a gray arrow).

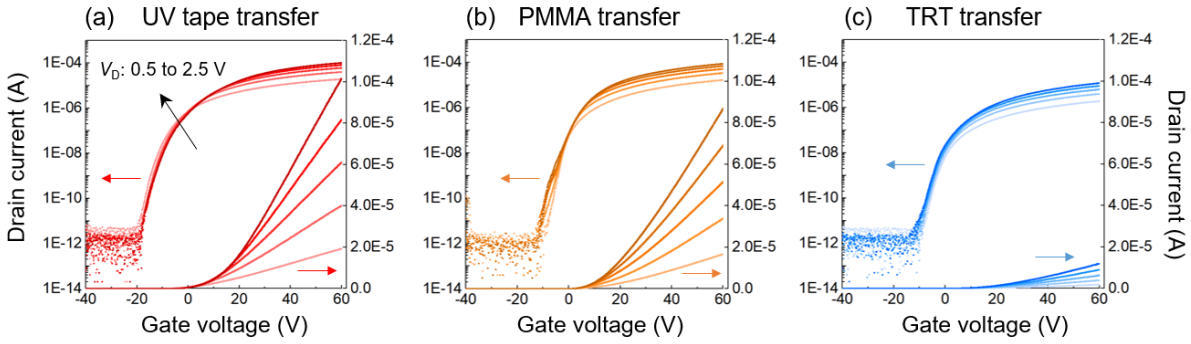

Supplementary Fig. 21. Comparison of the FET characteristics of MoS_2 FETs. Transfer curves of monolayer MoS_2 FETs made with the MoS_2 grains transferred with the UV tape (**a**), PMMA (**b**), and TRT (**c**). The electron mobilities are 23, 24, and 3 cm^2/Vs, respectively. The device measurement was performed in vacuum ($<10^{-4}$ Pa) at room temperature. It is seen that the threshold voltage is positively shifted in PMMA (**b**) and TRT (**c**) samples as compared with the UV tape sample (**a**), suggesting the p-type doping effect induced by the surface residues of PMMA and TRT.

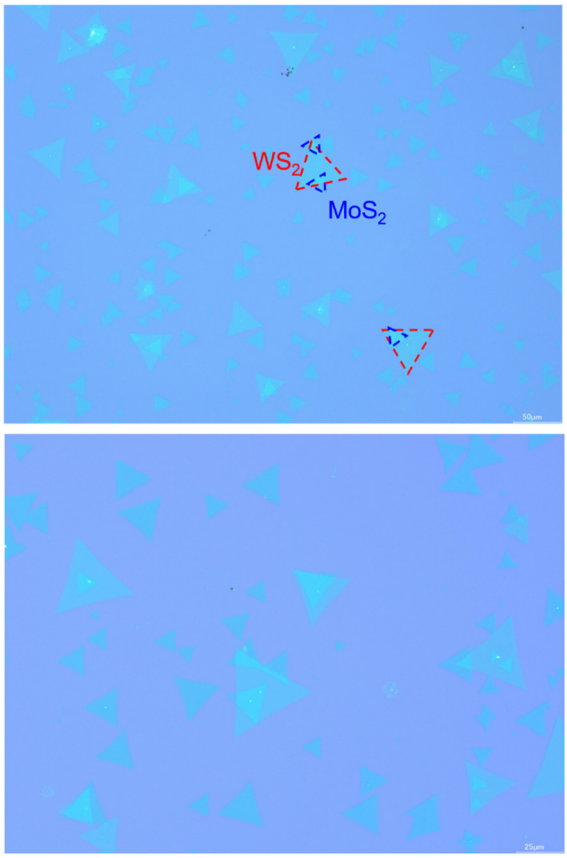

Supplementary Fig. 22. MoS_2/WS_2 stacked heterostructures made by the sequential tape transfer. Optical micrographs of the MoS_2/WS_2 heterostacks made by transferring WS_2 with a UV tape, followed by the transfer of MoS_2 using another tape. These images indicate that the tape transfer is very clean without tape residue, promoting the effective coupling between two materials.

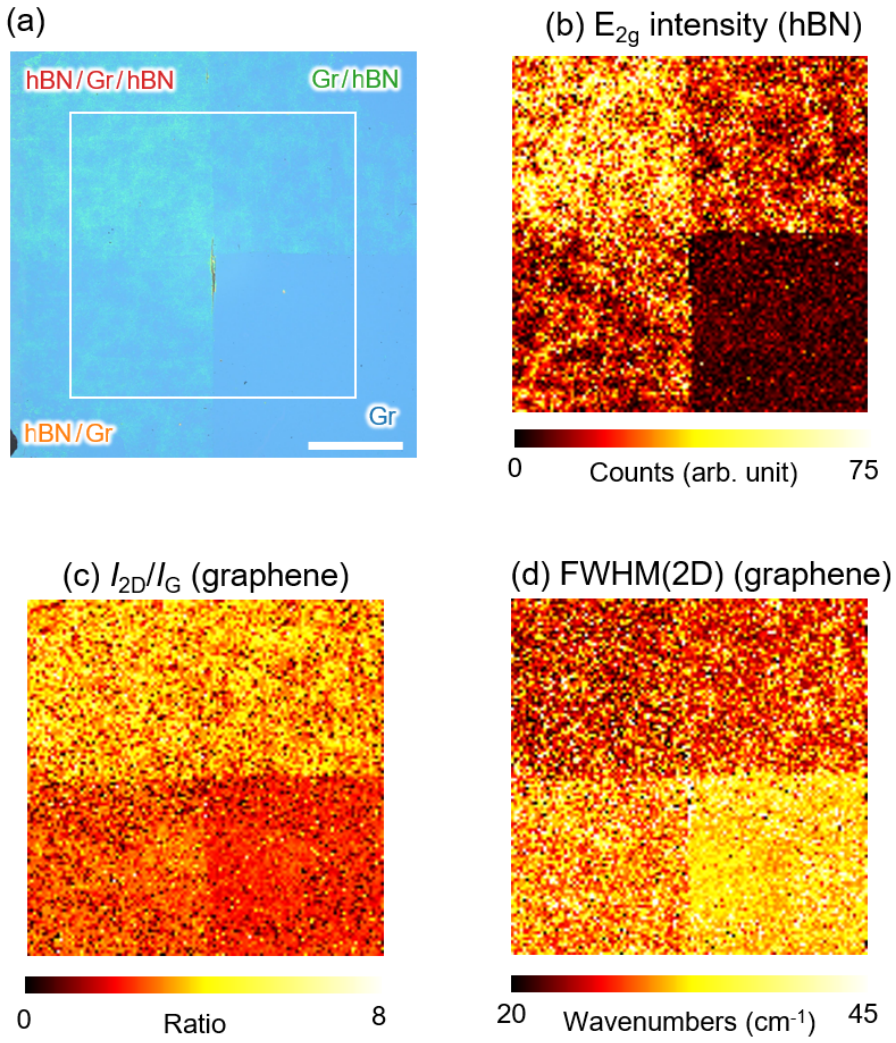

Supplementary Fig. 23. Wide-area Raman mapping of the graphene-hBN heterostacks. Large-area Raman mapping was performed for the areas shown in Fig. 4h. **a**, Optical image, with the area mapped by Raman highlighted by the white square. **b**, Raman mapping of the intensity of the hBN E_{2g} band. **c,** The intensity ratio of 2D band to G band of graphene. **d**, FWHM(2D) of the graphene. The Raman mapping measurements were performed inside the square shown in **a** with 50 μm step. Scalebar in **a** represents 2 mm.

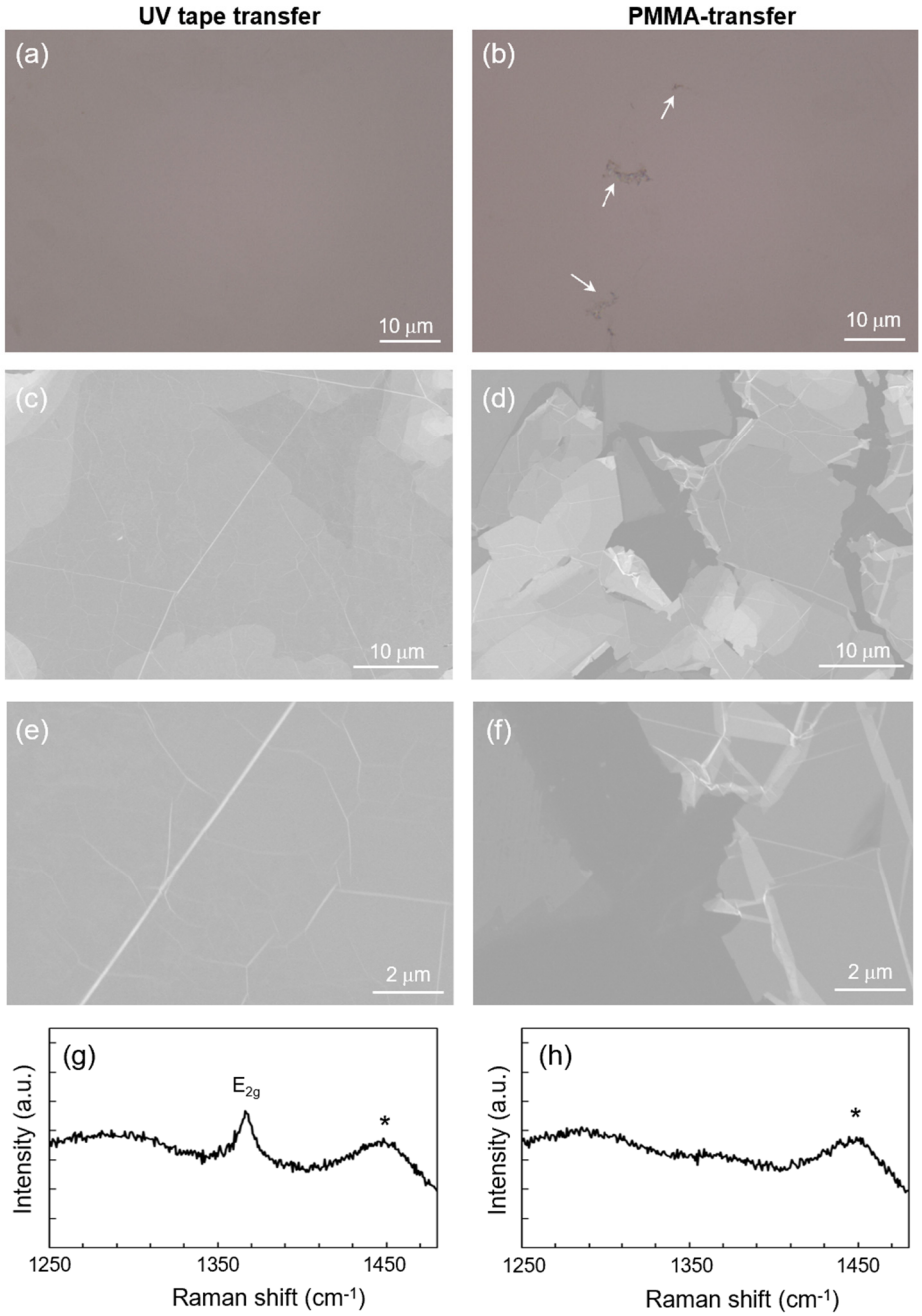

Supplementary Fig. 24. Comparison of the transfer of multilayer hBN on Si surface without a top SiO_2 layer. Optical images of multilayer hBN transferred on a Si substrate with UV tape (**a**) and PMMA (**b**). SEM images of multilayer hBN transferred on a Si substrate with UV tape (**c**,**e**) and PMMA (**d**,**f**). **g**,**h**, Raman spectra measured after the transfer. It is very difficult to transfer hBN on Si surface (without SiO_2) by PMMA, because the hBN detaches from the Si surface in the final PMMA dissolution step. In contrast, the UV tape method can transfer the hBN even on the Si substrate. Similar results were obtained for graphene transfer when Si substrate without a surface SiO_2 layer was used.

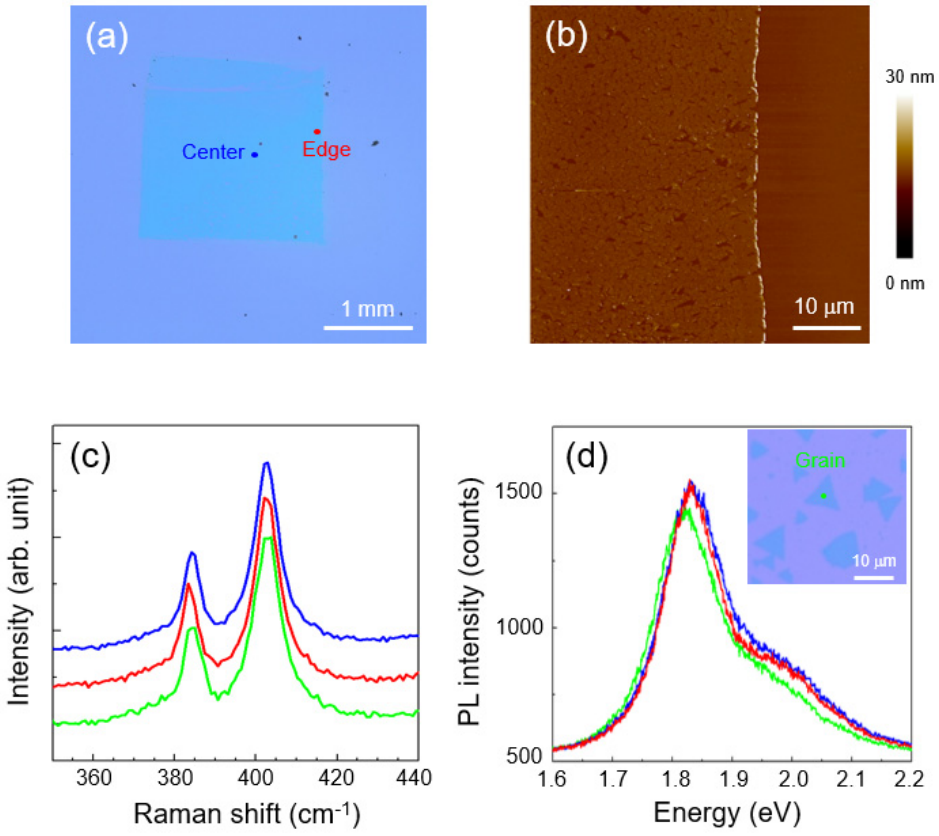

Supplementary Fig. 25. MoS_2 pattern prepared by the cut-and-transfer method. a, Optical image of one of the transferred MoS_2 pattern. **b**, AFM image of the pattern edge. Raman (**c**) and PL spectra (**d**) of the MoS_2 measured at the pattern edge (red) and center (blue) marked in **a**. The Raman spectrum of the isolated MoS_2 grain (green) is also shown for the sake of comparison, which was measured at the point marked in the inset of **d**. The MoS_2 pattern shows smooth edge, indicating that the pattern transfer can be done without deformation nor warping. The Raman and PL spectra indicate that there is no clear influence of mechanical strain at the pattern edge. Small holes in the MoS_2 pattern are originated in incomplete MoS_2 coverage during the CVD growth due to small grain sizes (~1 μm).

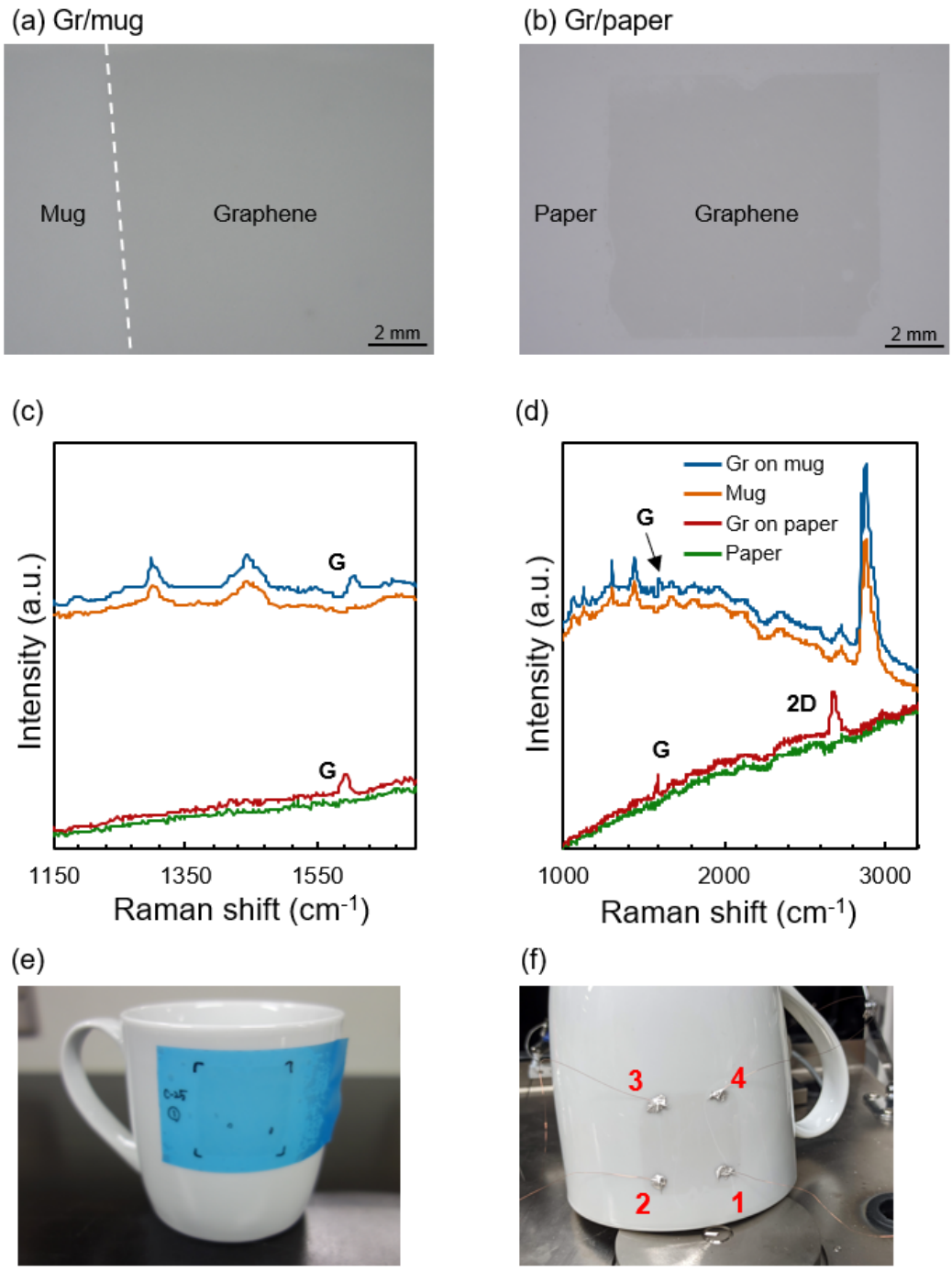

Supplementary Fig. 26. Monolayer graphene transferred on a ceramic mug and a piece of paper. a, Optical image of graphene on the ceramic mug shown in Fig. 6b. **b**, Optical image of graphene transferred on a sheet of paper using the UV tape. **c,d**, Raman spectra of the graphene on a mug and paper. **e**, Photograph of the tape/graphene/mug taken before removing the tape. **f**, Photograph of the graphene/cup with electrodes for electrical measurement. The sheet resistance was 71 kΩ/□.

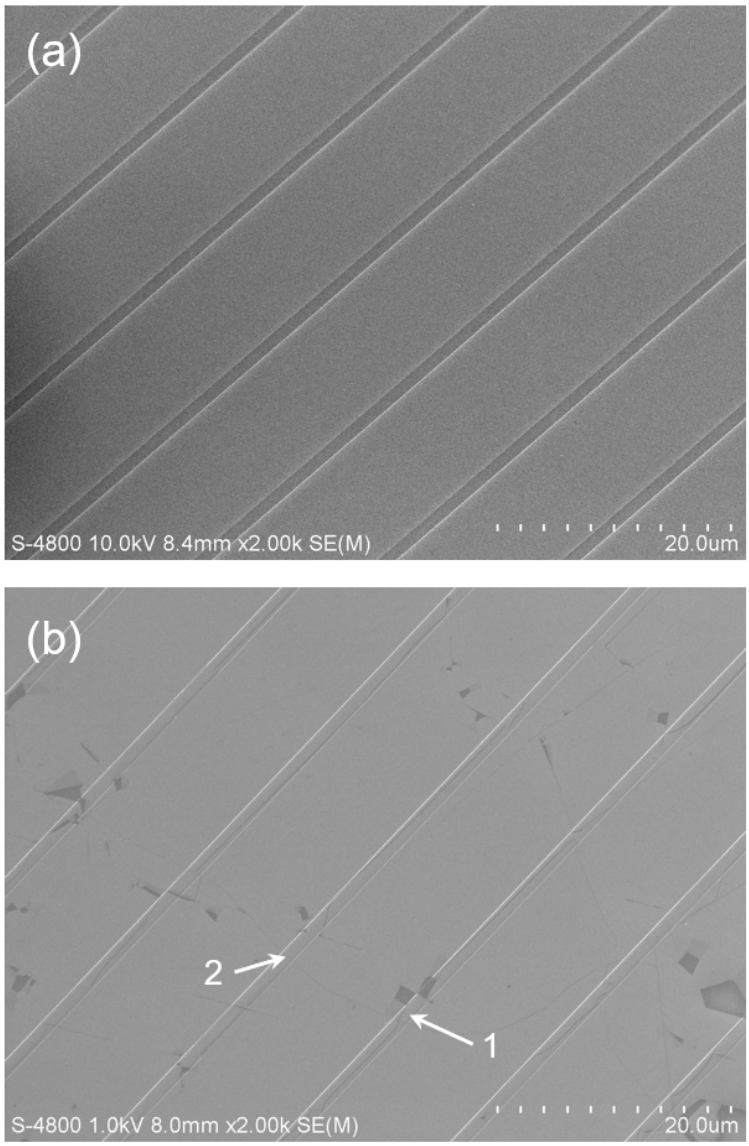

Supplementary Fig. 27. Transferred monolayer graphene on trenched surface. a, SEM image of the original SiO_2/Si substrate with trenches taken before the graphene transfer. **b**, SEM image of the transferred, monolayer graphene on the trenched SiO_2/Si substrate. Point 1 indicates the folded area. While the bare SiO_2 surface appears darker, the trench did not show such dark contrast. Point 2 shows a wrinkle crossing the trenches. These features prove that the graphene is suspended over the trenches.

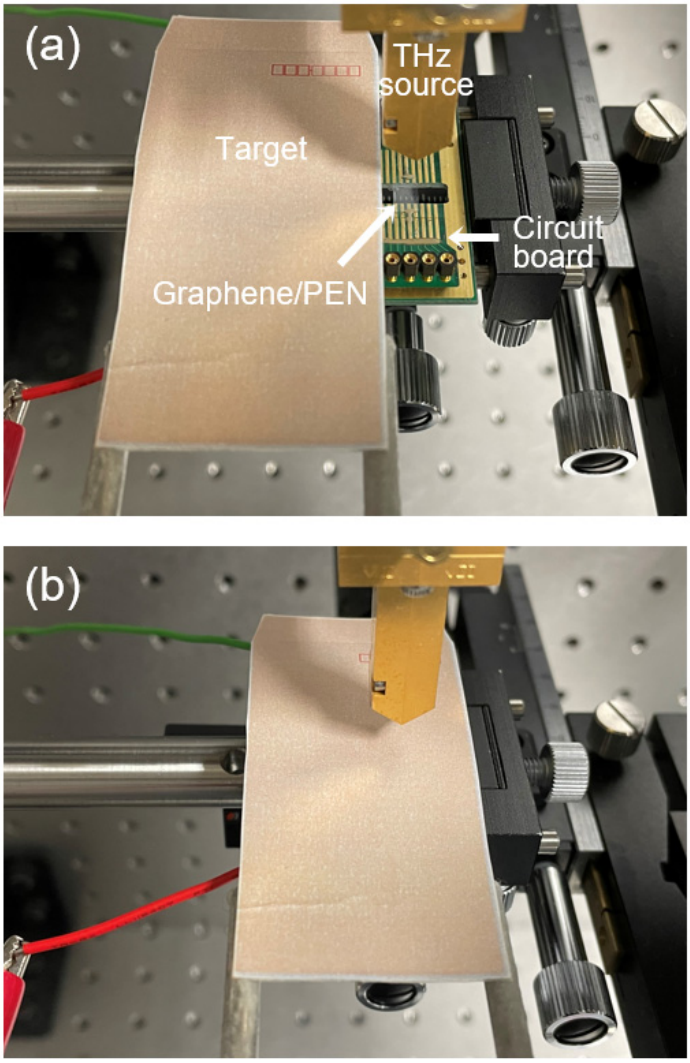

Supplementary Fig. 28. Experimental setup used for THz imaging. a, Setup used for the THz imaging with a graphene sensor. The monolayer graphene was transferred on a PEN substrate using the UV tape, followed by attaching electrodes. **b**, Photograph during the THz imaging. The envelope having a knife and a piece of paper inside was moved by a *x*-*y* stage controller while measuring the THz response using the graphene sensor.

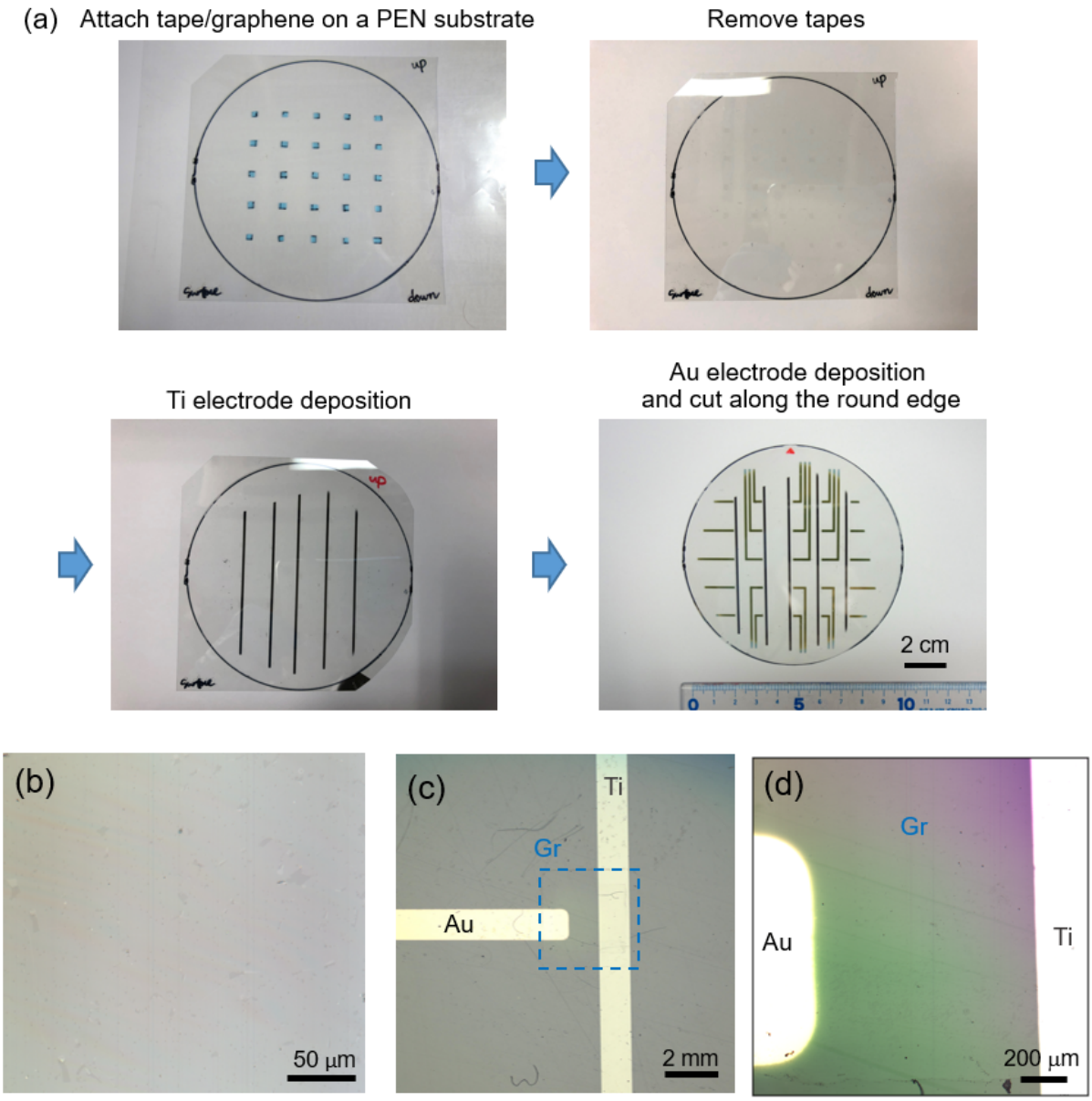

Supplementary Fig. 29. Fabrication of thermal imaging device array. a, Photographs showing each step of the device fabrication using small pieces of the graphene tapes. Two different electrodes, Ti and Au, were evaporated using metal masks with different designs. **b**, Optical image of graphene transferred on a PEN substrate. The presence of a graphene sheet can be recognized by small breaks. Here, we intentionally selected a damaged area to evidence the presence of graphene on the transparent PEN substrate. **c,d**, Optical images of the final device, in which each graphene piece was connected to Ti and Au electrodes.

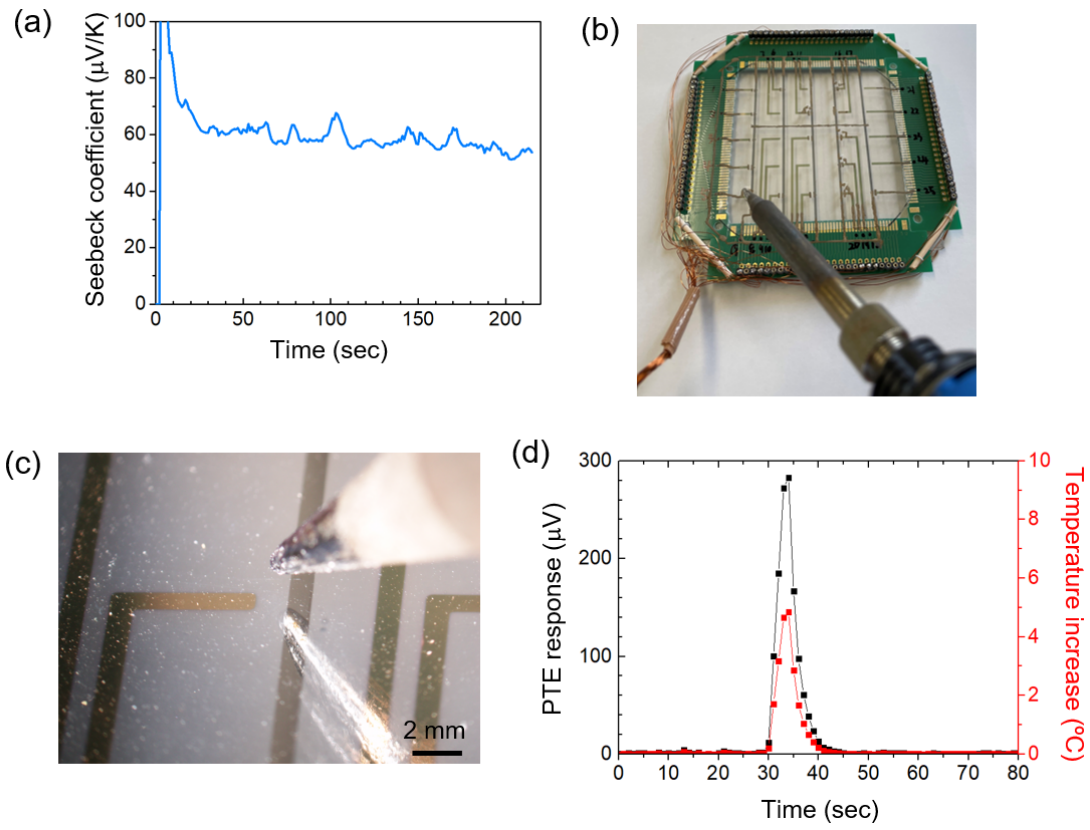

Supplementary Fig. 30. Fundamental behavior of the graphene device array. **a**, Seebeck coefficient of a monolayer graphene device. **b,** Photograph of the device array during the measurement using the soldering iron rod. **c**, Zoomed image of the tip of the soldering iron rod during the thermal imaging measurement. **d,** Passive photo-thermoelectric (PTE) response and the estimated temperature change of the graphene sensor located below the soldering iron rod.

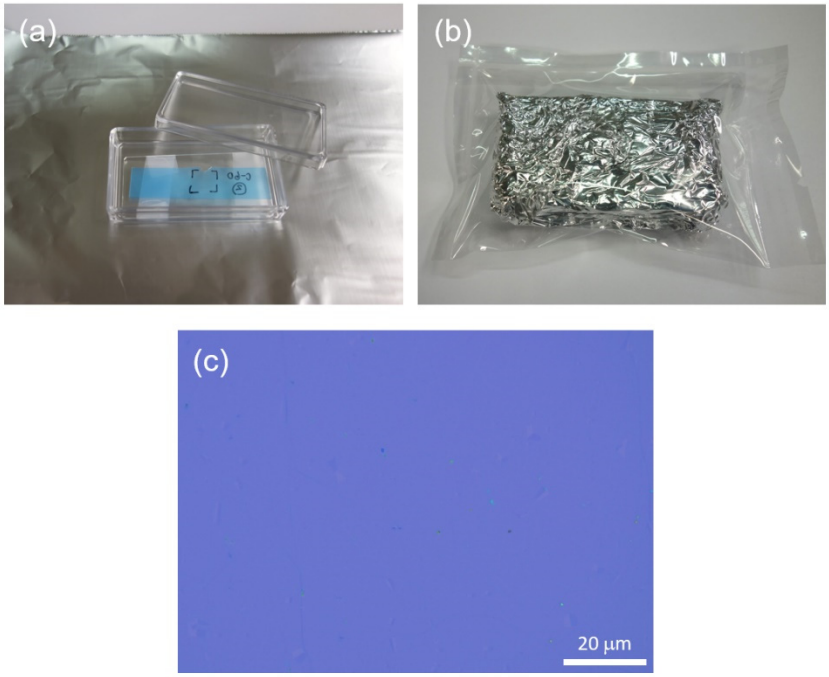

Supplementary Fig. 31. Long time storage of the UV tape/graphene stack. **a**, The tape/graphene stack just after the electrochemical transfer. **b**, The stack was stored in N_2 gas environment in dark for one month. **c**, Optical image of the monolayer graphene transferred after one-month storage.

Supplementary Table 1. XPS elemental analysis data of the surfaces of UV tape and graphene. XPS was measured for the UV tape surface, graphene/Cu(111)/sapphire, and after the graphene transfer on SiO_2. The absence of N atoms on the graphene surface after the transfer process proves the clean transfer without tape residue on the graphene surface. "—" indicates the peak intensity was below the detection limit (<0.1atm% for Cu, and <0.2 atm% for N and Si atoms). Other elements, such as S, Cl, Sn, were note detected.

		C	N	O	Si	Cu
UV tape surface	Batch 1	65.5	5.5	29.0	—	—
	Batch 2	64.9	5.5	29.6	—	—
Graphene/Cu/Al_2O_3 (before transfer)	Batch 1	51.5	—	11.5	1.1	35.9
	Batch 2	51.8	—	11.6	1.2	35.4
Graphene/SiO_2 (after transfer)	Batch 1	40.4	—	39.9	19.7	—
	Batch 2	40.1	—	40.8	19.1	—

Supplementary Table 2. Details of the UV tapes used to transfer 2D materials.

Material		**Graphene**	**TMDs, hBN**
Adhesive layer	Copolymer	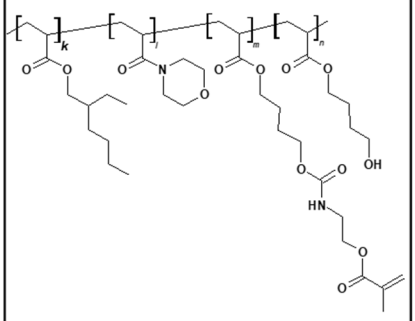	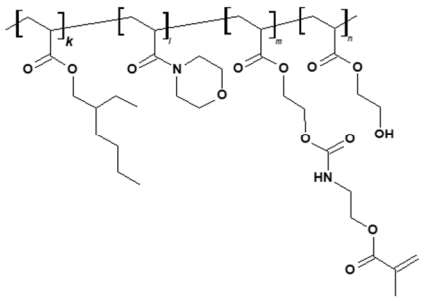
		2-Ethylhexyl acrylate 4-Acryloylmorpholine 4-hydroxybutyl acrylate (partly reacted with 2-isocyanatoethyl methacrylate)	2-Ethylhexyl acrylate 4-Acryloylmorpholine 2-hydroxyethyl acrylate (partly reacted with 2-isocyanatoethyl methacrylate)
	Cross-linking agent	Coronate L (Tosoh)	Coronate L (Tosoh)
	Photoinitiator	Omnirad651 ~6wt% (IGM Resins B.V.)	Omnirad651 ~3wt% (IGM Resins B.V.)
	Thickness (μm)	30	15
Substrate		Polyolefin ~100 μm	Polyolefin ~100 μm

Preparation of the UV tapes.

1. UV tape used for the graphene transfer

In a round bottom flask, 2-ethylhexyl acrylate (60 mol), 4-acryloylmorpholine (40 mol), 4-hydroxybutyl acrylate (22 mol) were added. In this solution, benzoyl peroxide (0.2 weight part against the above solution) and ethyl acetate (65 weight part) were added, followed by heating at 61 °C for 6 hours in N_2 gas to make a random copolymer. In this copolymer solution, 2-methacryloyloxyethyl isocyanate (2.2 mol) was added and heated at 50 °C for 48 hours to convert to acrylic polymer. Then, an isocyanate cross-linking agent (12 weight part, Coronate L, Tosoh Co.) and photoinitiator (6 weight part, Omnirad651, IGM Resins B.-V.) were mixed and used as an adhesive layer.

The obtained adhesive was coated on a silicone-coated polyethylene terephthalate (PET) film, followed by heating at 130 °C for 3 minutes in air. The thickness of this adhesive layer was ~30 μm. Finally, the adhesive layer was attached to a polyolefin substrate with a thickness of ~100 μm for the use of graphene transfer.

2. UV tape used for TMD and hBN transfer

In a round bottom flask, 2-ethylhexyl acrylate (75 mol), 4-acryloylmorpholine (25 mol), 4-hydroxybutyl acrylate (22 mol) were added. In this solution, benzoyl peroxide (0.2 weight part against the above solution) and ethyl acetate (65 weight part) were added, followed by heating at 61 °C for 6 hours in N_2 gas to make a random copolymer. In this copolymer solution, 2-methacryloyloxyethyl isocyanate (11 mol) was added and heated at 50 °C for 48 hours to convert to acrylic polymer. Then, an isocyanate cross-linking agent (4 weight part, Coronate L, Tosoh Co.) and photoinitiator (3 weight part, Omnirad651, IGM Resins B.-V.) were mixed and used as an adhesive layer.

The obtained adhesive was coated on a silicone-coated PET film, followed by heating at 130 °C for 3 minutes in air. The thickness of this adhesive layer was ~15 μm. Finally, the adhesive layer was attached to a polyolefin substrate with a thickness of ~100 μm for the use of TMD and hBN transfer.

Supplementary Table 3. DFT result of the physisorption of two monomers and one dimer on the graphene surface using the model shown in Fig. 3b,c.

	Vertical distance (nm)	E_{ad} (eV)[a)]	ΔE_{disp} (eV)[b)]	Maximum adhesion force (nN)
monomer	0.343	0.925	1.063	0.882
dimer	0.395	0.688	0.750	0.664

a) The adsorption energy (E_{ad}) was estimated from the Morse potential approximation.
b) The total energy (E_{tot}) of the system can be decomposed into the contributions from the DFT energy (E_{DFT}) and the dispersion energy (E_{disp}):
$E_{tot} = E_{DFT} + E_{disp}$
ΔE_{disp} was estimated from the difference in dispersion energy before and after the adhesion.

Supplementary Table 4. Comparison of the device performance of CVD-grown monolayer MoS_2. The number in the parentheses shows the highest mobility. Note that the carrier mobility depends not only on the quality of the transferred MoS_2 but also on device structure (such as electrode metals) and channel size.

Number of layers	Growth substrate	Transfer method	Carrier mobility (cm^2/Vs)	On/off ratio	Ref.
1L	sapphire	UV tape + water	8.5 (23)	$>10^6$	This work
1L	sapphire	NA	0.003–0.03	NA	1
1L	sapphire	Polystyrene (PS) + water	0.03	NA	2
1L	sapphire	PMMA + KOH_{aq}	~25 (43)	NA	3
1L	sapphire	PMMA + $NaOH/NaF_{aq}$	0.1–1	10^6	4
1L	sapphire	Polydimethylsiloxane (PDMS) + water	40	10^6	5
1L	sapphire	PMMA + KOH_{aq}	1.2	$\sim10^5$	6
1L	sapphire	PMMA + KOH_{aq}	78 (103)	10^8	7
1L	SiO_2/Si	–	0.23	10^5	8
1L	SiO_2/Si	–	10.5	10^7	9
1L	SiO_2/Si	PMMA + KOH_{aq} (transferred on another SiO_2/Si)	45	10^6	10

References

(1) Yu, Y. et al. *Sci. Rep.* **3**, 1866 (2013).
(2) Gurarslan, A. et al. *ACS Nano* **8**, 11522 (2014).
(3) Dumcenco, D. et al. *ACS Nano* **9**, 4611 (2015).
(4) Ji, Q. et al. *Nano Lett.* **15**, 198 (2015).
(5) Yu, H. et al. *ACS Nano* **11**, 12001 (2017).
(6) Durairaj, S. et al. *Nanoscale Adv.* **2**, 4106 (2020).
(7) Li, T. et al. *Nat. Nanotechnol*. **16**, 1201 (2021).
(8) Zhang, W. et al. *Adv. Mater.* **25**, 3456 (2013).
(9) Liu, H. et al. *Nano Lett.* **13**, 2640 (2013).
(10) Schmidt, H. et al. *Nano Lett.* **14**, 1909 (2014).